PHYSICAL REVIEW D **92,** 015019 (2015)

Laboratory-frame observables for probing the top-Higgs boson interaction

Fawzi Boudjema[*] and Diego Guadagnoli[†]
LAPTh, Université de Savoie Mont Blanc et CNRS, BP110, F-74941 Annecy-le-Vieux Cedex, France

Rohini M. Godbole[‡]
CHEP, Indian Institute of Science, Bangalore 560012, India

Kirtimaan A. Mohan[§]
Department of Physics and Astronomy, Michigan State University, East Lansing, Michigan 48824, USA
(Received 13 May 2015; published 21 July 2015)

We investigate methods to explore the CP nature of the $t\bar{t}h$ coupling at the LHC, focusing on associated production of the Higgs boson with a $t\bar{t}$ pair. We first discuss the constraints implied by low-energy observables and by the Higgs-rate information from available LHC data, emphasizing that they cannot provide conclusive evidence on the nature of this coupling. We then investigate kinematic observables that could probe the $t\bar{t}h$ coupling directly, in particular, quantities that can be constructed out of just *laboratory-frame* kinematics. We define one such observable by exploiting the fact that $t\bar{t}$ spin correlations do also carry information about the CP nature of the $t\bar{t}h$ coupling. Finally, we introduce a CP-odd quantity and a related asymmetry, able to probe CP violation in the $t\bar{t}h$ coupling and likewise, constructed out of laboratory-frame momenta only.

DOI: 10.1103/PhysRevD.92.015019 PACS numbers: 12.60.Fr, 14.65.Ha, 14.80.Ec

I. INTRODUCTION

The 7–8 TeV runs of the LHC have led to the discovery of a scalar particle with a mass $m_h \simeq 125$ GeV [1–4]. The properties measured so far show very good consistency with those expected for the Standard-Model (SM) Higgs boson. Further, these runs have not revealed the existence of new particles. The fact remains that the SM cannot address a few pressing questions, such as the baryon asymmetry of the universe, the large mass hierarchy in the fermion sector as well as an explanation for the dark matter abundance in the Universe. These issues call for new physics (NP) beyond the SM. Furthermore, the observation of a 125 GeV *elementary* scalar, as well as the absence so far of NP at the TeV scale, leave unanswered the question of why its mass m_h is so different than the gravitational scale.

In order to ease the explanation of the observed baryon asymmetry, new sources of CP violation are desirable. Such sources exist in many simple extensions of the SM. One notable example is an extended Higgs sector such as a two Higgs doublet model. Therein, CP violation is incorporated in the Higgs sector through mixing of CP-even and -odd states. Within these models, the 125-GeV boson identified with the Higgs boson can have indefinite CP quantum numbers due to mixing of CP-even and -odd states. A determination of the CP nature of this particle and its interactions may thus hold a clue of NP.

A program to probe the CP nature of the discovered Higgs scalar is already under way at the LHC experiments. The pure pseudoscalar hypothesis has already been ruled out at greater than 95% confidence level (C.L.) and consistency with the CP-even nature established by ATLAS [5] and CMS [6,7] Collaborations. This has been achieved by an analysis of the hZZ coupling using $(h \to Z^{(*)}Z^{(*)})$ decay channel.[1] It should be noted however that tree-level coupling of the CP-odd component of the Higgs boson to gauge bosons is in fact not allowed and can only proceed through loops. Couplings between the Higgs CP-odd component and gauge bosons manifest themselves as operators of dimension six (or higher) in the language of effective Lagrangians. The effect of such operators is expected to be suppressed in comparison to tree-level interactions.

On the other hand, the CP-odd component of the Higgs boson couples to fermions at the tree level. As a result, the Higgs-fermion couplings provide an unambiguous and more sensitive probe of a CP-mixed state compared to Higgs-gauge-boson couplings.[2] It is possible to probe Higgs-fermion couplings by studying Higgs decays to

[*]fawzi.boudjema@lapth.cnrs.fr
[†]diego.guadagnoli@lapth.cnrs.fr
[‡]rohini@cts.iisc.ernet.in
[§]kamohan@pa.msu.edu

[1]For discussions of the $(h \to Z^{(*)}Z^{(*)})$ decay mode as a probe of the Higgs CP properties see, for example, Refs. [8–17]. It is also possible to probe the same in vector boson fusion [18–23] production and associated Higgs vector boson (Vh) production [24–30].

[2]Note that the Higgs boson to diphoton decay proceeds through loop processes at leading order (LO) (unlike decays to W and Z bosons), making it sensitive to the CP-odd component of the Higgs boson.

fermions. Since these are two-body decays of a spin 0 particle, the *CP* nature of the coupling is reflected in the spin correlation of the decay fermions. Luckily, the spin information of the t, τ is also reflected in the decay products of the same. This as well as their larger couplings, offers possibilities of probing the *CP* nature of the Higgs boson through an analysis of the $h\tau\bar{\tau}$ and $ht\bar{t}$ coupling. Analysis of this coupling using the $h \to \tau\bar{\tau}$ case has been shown to be quite promising for this purpose [31–34]. However, a measure of the strength of the coupling *CP*-odd component in the $h\tau\tau$ interaction does not automatically qualify as a measure of the same for other fermions, i.e., the *CP*-odd component may not couple to all fermions universally (as is the prediction in some NP models). It therefore becomes important to be able to probe the *CP* nature of the Higgs boson in all its couplings. The largest of all such couplings, $t\bar{t}h$, cannot be tested by direct decay, because $h \to t\bar{t}$ is not allowed. However, the large value of this coupling implies large production rates for associated production of the Higgs boson with a $t\bar{t}$ pair, and this mode therefore qualifies as the most direct probe of the Higgs-top coupling and of the *CP* nature of the Higgs boson.

Also from a more general perspective, it is well-known that the coupling of the Higgs boson to the top quark is of great relevance, theoretically and experimentally alike. On the theoretical side, the importance of the top Yukawa coupling follows from the fact that it is numerically very close to unity. Such a large value of the Yukawa coupling is suggestive of an active role of the top quark in the generation of the electroweak-symmetry breaking (EWSB) scale. As a matter of fact, the Higgs-top interaction has important consequences on spontaneous symmetry breaking within the SM—notably, on vacuum stability arguments—as well as beyond the SM—where the top drives electroweak symmetry breaking in some scenarios. Most importantly, this coupling drives the main production channel at the LHC (gluon fusion), and also contributes to the crucial decay of the Higgs boson into two photons.

The above considerations justify the importance of measuring the top-Higgs coupling with the highest accuracy achievable, and, in particular, of determining it by *direct measurement* via $t\bar{t}h$ production. In this paper, we focus on this possibility.

We parametrize the Higgs couplings to fermions through the effective Lagrangian

$$\mathcal{L}_{hf\bar{f}} = -\sum_f \frac{m_f}{v} h\bar{f}(a_f + ib_f\gamma_5)f, \qquad (1)$$

where the sum is over all quarks and leptons. In the SM, where the Higgs boson is a scalar, $a_f = 1$ and $b_f = 0$ for any fermion f. For a pure pseudoscalar $a_f = 0$ and $b_f \neq 0$. A Higgs boson with mixed *CP* properties is realized if both $a_f \neq 0$ and $b_f \neq 0$. The exact values of these coefficients will depend on the specific model. Here we are interested in a model-independent approach to determine, from data, the nature of the $t\bar{t}h$ interaction which is potentially the largest coupling of all fermions.

The production and decay rates of the Higgs boson measured at the LHC [35–37] do provide important constraints on the strength of both a_t, b_t. Indirect constraints will be discussed in more detail in Sec. II, with the aim of spelling out the underlying assumptions that enter the derivations of these constraints. We will show that strong constraints on a_t and b_t can be placed *only* under these assumptions.

As argued, the most general and direct determination of the a_t, b_t couplings in Eq. (1) is possible by measuring $t\bar{t}h$ production.[3] The $t\bar{t}h$ production mode is notoriously hard to measure at the LHC, yet feasible. In fact, already with the limited data set of the 7 and 8 TeV runs of the LHC, the signal strengths in the $t\bar{t}h$ production channel have been measured by both ATLAS [48,49] and CMS [50] Collaborations. Some preliminary studies suggest that a significant ($> 5\sigma$) measurement of Higgs production in the $t\bar{t}h$ channel is possible for upcoming runs of the LHC [51–57].

Needless to say, a measurement of the $t\bar{t}h$ production cross section alone is not sufficient to determine the vertex in Eq. (1) completely. To this end, it is necessary to consider in detail the $t\bar{t}h$ production and the decay kinematics. In this paper, we suggest and discuss useful discriminating observables to probe the vertex in Eq. (1), with emphasis on those that can be defined directly in the laboratory frame. Note that, on the other hand, we refrain from entering the discussion about a precision determination of the vertex.

The rest of this paper is organized as follows. In Sec. II, we describe and derive indirect constraints on the couplings a_t and b_t. In Sec. III, we then proceed to analyze $t\bar{t}h$ production at the LHC and construct various observables, including a *CP*-violating one, that could be used to determine the nature of the $t\bar{t}h$ interaction itself. Finally in Sec. IV, we summarize and conclude.

II. INDIRECT PROBES OF AN ANOMALOUS $t\bar{t}h$ COUPLING

Electric dipole moments (EDMs) can impose severe constraints on new *CP*-violating weak phases. A scalar with mixed parity that couples to both the electron and the top as described by Eq. (1) leads to *CP* violation through interference of the type $a_f b_{f'}$. Indeed at a two-loop, a Barr-Zee type diagram induces an EDM for the electron of the form $d_e \propto b_t a_e f_1(m_t^2/m_h^2) + b_e a_t f_2(m_t^2/m_h^2)$, where a_e, b_e have been defined in Eq. (1), and $f_{1,2}$ are known loop functions [58]. Under the assumption that the

[3]An alternative approach, which we do not discuss in this work, to study the couplings in Eq. (1), is to use single top production [38–47].

Higgs-electron coupling is standard, $a_e = 1, b_e = 0$, a rather stringent constraint, $b_t < 0.01$, can be realized [59]. Of course, with different assumptions on a_e, b_e, or even with additional sources of CP violation, this constraint can become milder or evaporate altogether. For example, and as emphasized in Ref. [59], current Higgs data are actually compatible with a Higgs boson only coupled to third-generation fermions. In this case, b_t values of O(1) are allowed by the EDM constraints. Furthermore, Ref. [60] provides another example of multi-Higgs scenario, realized in the framework of a CP violating supersymmetric model, in which the current EDM constraints can be satisfied, in spite of CP violating couplings between the Higgs states and the top quark.

It should be noted that, given the smallness of the electron Yukawa coupling, it is unclear whether the a_e, b_e couplings will be accessible experimentally in the near future. In order to reconstruct the $t\bar{t}h$ coupling direct probes of the same are necessary, which we will discuss in the next section. In this section, we focus our attention on the constraints on the $t\bar{t}h$ coupling that can be derived from Higgs rate information collected at the LHC. We will show that these constraints strongly depend on the nature of the assumption and one cannot conclusively determine the $t\bar{t}h$ vertex using signal strengths alone.

A. Constraints from measurements of Higgs rates

Within the SM, and with Higgs and top masses as measured, there are four main production modes of the Higgs bosons at the LHC: gluon fusion (ggF), vector-boson fusion (VBF), Higgs production in association with a W/Z boson (Vh), and Higgs production in association with a $t\bar{t}$ pair. The gluon-fusion production mode has the largest cross section at the LHC, and the dominant contribution to this process comes from a top loop. The Higgs decay to two photons has also a contribution due to a top loop, although the dominant one comes from a W-boson loop. ATLAS and CMS Collaborations have already put indirect constraints on the value of a_t in Eq. (1), assuming that there are no other sources contributing to the effective couplings $gg \to h$ or $h \to \gamma\gamma$. At a 95% confidence level, these constraints read [61,62]

$a_t \in [-1.2, -0.6] \cup [0.6, 1.3]$	ATLAS Collaboration
$a_t \in [0.6, 1.2]$	CMS Collaboration.

In this section, we extend this analysis by allowing in the fit both a_t and b_t couplings in Eq. (1), and by including the recently measured $t\bar{t}h$ channel signal strengths [48–50,63,64]. Higgs couplings to massive gauge bosons are defined by

$$\mathcal{L}_{hVV} = g m_W h \left(\kappa_W W^\mu W_\mu + \frac{\kappa_Z}{2\cos\theta_w^2} Z^\mu Z_\mu \right). \quad (2)$$

In the SM and at tree level, $\kappa_Z = \kappa_W = \kappa_V = 1$. As customary, the signal strength measured in a particular channel i at the LHC is defined as

$$\hat{\mu}_i = \frac{n^i_{\rm exp}}{n^i_{\rm SM}}, \quad (3)$$

where $n^i_{\rm exp}$ is the number of events observed in the channel i and $n^i_{\rm SM}$ is the expected number of events as predicted in the SM. In order to contrast specific model predictions with the experimentally derived $\hat{\mu}_i$, we define (as usual)

$$\mu_i = \frac{n^i_{\rm th}}{n^i_{\rm SM}} = \frac{\Sigma_p \sigma_p \epsilon^i_p}{\Sigma_p \sigma^{\rm SM}_p \epsilon^i_p} \times \frac{\mathcal{B}_i}{\mathcal{B}^{\rm SM}_i}. \quad (4)$$

Here, $n^i_{\rm th}$ corresponds to the expected number of events predicted in the hypothesized model under consideration; σ_p corresponds to the cross section in the $p^{\rm th}$ production mode, i.e., the cross section for Higgs production in one of the four production modes listed earlier; $\mathcal{B}_i$ is the branching ratio of the Higgs boson in the $i^{\rm th}$ channel; ϵ^i_p is the efficiency of the $p^{\rm th}$ production mode to the selection cuts imposed in the $i^{\rm th}$ channel. Note that the efficiencies in the numerator and denominator of Eq. (4) are taken to be the same. This is true at the leading order for the gluon fusion process.

In order to evaluate the signal strength in the $t\bar{t}h$ production channel, ATLAS [48,49,63–65] and CMS [50] Collaborations first apply some basic selection cuts and then use boosted decision trees (BDT) to further separate the signal from the background. We have checked at the parton level that for basic selection cuts, the efficiency in the two cases of pure scalar vs pure pseudoscalar Higgs bosons are not significantly different. However, this may not be the case for BDT. We neglect this effect here, we namely assume that BDT analyses will have the same efficiency for a scalar and a pseudoscalar Higgs boson and set them to be equal.

We next discuss the a_t and b_t coupling contributions to Higgs production from gluon fusion and Higgs decay to two photons. The ratio of the Higgs decay width to two photons to the SM decay width, at next to leading order and neglecting the small contribution from fermions other than the top quark, can be written in the form [66,67]

$$\frac{\Gamma(h\to\gamma\gamma)}{\Gamma(h\to\gamma\gamma)^{\rm SM}} \simeq \frac{|\kappa_W A_W^a(\tau_W)+\frac{4}{3}a_t(1-\alpha_s/\pi)A_t^a(\tau_t)|^2+|\frac{4}{3}b_t A_t^b(\tau_t)|^2}{|A_W^a(\tau_W)+\frac{4}{3}(1-\alpha_s/\pi)A_t^a(\tau_t)|^2}$$
$$\simeq 1.6((\kappa_W-0.21a_t)^2+0.12b_t^2). \quad (5)$$

Here, A_j^i denote the loop functions due to the W loop (A_W^a), the CP-even top coupling (A_t^a) and its CP-odd counterpart (A_t^b). The analytical expressions for these functions are given in Appendix B. It should be stressed that, given the measured Higgs and top masses, implying $\tau_t = m_h^2/(4m_t^2) \ll 1$, the top contribution (both scalar and pseudoscalar) is, to a very good approximation, given by its expression in the infinite top-mass limit (see Appendix B). Correspondingly, α_s corrections are included in this limit. In the same limit, they affect only the scalar contributions, whereas the pseudoscalar one is untouched.

We relate Higgs production through gluon fusion, normalized to the SM value, to the corresponding normalized width of Higgs bosons to two gluons. Keeping only the dominant top contribution again, we may write,[4]

$$\frac{\sigma(gg\to h)}{\sigma(gg\to h)^{\rm SM}} \simeq \frac{\Gamma(h\to gg)}{\Gamma(h\to gg)^{\rm SM}}$$
$$\simeq a_t^2 + b_t^2\frac{|A_t^b(\tau_t)|^2}{|A_t^a(\tau_t)|^2}\left(1+\frac{1}{2}\frac{\alpha_s}{\pi}\right)$$
$$\simeq a_t^2 + 2.29 b_t^2. \quad (6)$$

Note that, the indirect effect of the pseudoscalar contribution in $gg\to h$ (and $h\to gg$) is more than twice the corresponding scalar contribution (with $a_t = b_t$). As we will see, in direct $t\bar{t}h$ production, it is the scalar that contributes the most.

We now perform a global fit to the Higgs data collected by the ATLAS Collaboration, CMS Collaboration, and Tevatron in order to estimate the allowed values of a_t and b_t. We follow closely the procedures of Refs. [35,36,68].

In general, BSM models allow for additional interactions not present in the SM to both the scalar and pseudoscalar components of the Higgs boson, that may be CP conserving or not. Gluon fusion and Higgs boson to diphoton decays, being loop-induced processes, are sensitive probes of this new physics. In this sense, unknown heavy physics not related to the top could contribute to the effective operators describing gluon fusion ($hG^{\mu\nu}G_{\mu\nu}, hG^{\mu\nu}\tilde{G}_{\mu\nu}$, where $G_{\mu\nu}$ is the gluon field strength and $\tilde{G}_{\mu\nu}$ its dual) and decays into photons ($hF^{\mu\nu}F_{\mu\nu}$, $hF^{\mu\nu}\tilde{F}_{\mu\nu}$, $F_{\mu\nu}$ and $\tilde{F}_{\mu\nu}$ denoting again the electromagnetic field strength and its dual, respectively). In order to account for these additional BSM effects, following Ref. [68], we introduce four extra parameters κ_{gg}, $\tilde{\kappa}_{gg}$, $\kappa_{\gamma\gamma}$, and $\tilde{\kappa}_{\gamma\gamma}$ so that Eqs. (5) and (6) are modified as follows

$$\Gamma_{\gamma\gamma}/\Gamma_{\gamma\gamma}^{\rm SM} \simeq 1.6((\kappa_W - 0.21(a_t+\kappa_{\gamma\gamma}))^2 + 0.12(b_t+\tilde{\kappa}_{\gamma\gamma})^2),$$
$$\Gamma_{gg}/\Gamma_{gg}^{\rm SM} \simeq (a_t+\kappa_{gg})^2 + 2.29(b_t+\tilde{\kappa}_{gg})^2. \quad (7)$$

Note namely that the couplings κ_{gg}, $\tilde{\kappa}_{gg}$, $\kappa_{\gamma\gamma}$, and $\tilde{\kappa}_{\gamma\gamma}$ are normalized so that, in these observables, they shift a_t and b_t with a relative factor of unity.

The fit to μ_i is performed by minimizing the χ^2 function defined as

$$\chi^2 = \sum_i \left(\frac{\mu_i - \hat{\mu}_i}{\hat{\sigma}_i}\right)^2, \quad (8)$$

where $\hat{\mu}_i$ are the experimental measurements and $\hat{\sigma}_i$ their uncertainties. We take into account the possibility of asymmetric errors by using the prescription of Ref. [69]. Namely, whenever errors are quoted as $(\hat{\mu}_i)^{+y}_{-z}$, we take $\hat{\sigma}_i = y$ if $(\mu_i - \hat{\mu}_i) > 0$, and $\hat{\sigma}_i = z$ if $(\mu_i - \hat{\mu}_i) < 0$ [69]. In some of the measured channels, the experimental collaborations have provided information on the correlation between different production modes. In this case, we modify the χ^2 function to include these correlations as follows

$$\chi^2(i,j) = \frac{1}{1-\rho^2}\left[\left(\frac{\mu_i-\hat{\mu}_i}{\hat{\sigma}_i}\right)^2 + \left(\frac{\mu_j-\hat{\mu}_j}{\hat{\sigma}_j}\right)^2 - 2\rho\left(\frac{\mu_i-\hat{\mu}_i}{\hat{\sigma}_i}\right)\left(\frac{\mu_j-\hat{\mu}_j}{\hat{\sigma}_j}\right)\right], \quad (9)$$

where ρ is the correlation coefficient, and i and j correspond to different Higgs production modes. The data used in the fits are detailed in Tables I–VI in Appendix A.

1. Results

We first perform a fit to the SM couplings a_f and κ_V, while setting all other couplings to zero. The results of this fit are displayed in Fig. 1. Here, we only show the contours

[4]The first equality in Eq. (6), relating the widths and the cross section, is an exact equality at LO. Luckily, in the heavy top-mass limit ($m_h^2 \ll 4m_t^2$) and because we are considering ratios of $\sigma(gg\to h)$ and ratios of $\Gamma(h\to gg)$, the equality holds to a very good approximation also beyond LO. In particular, for the cross section, the higher-order long-distance corrections involving (infrared or collinear) emission are universal in this limit. There only remains a genuine higher-order correction which depends specifically on the nature of the $t\bar{t}h$ coupling. A large part of this finite regular correction cancels when considering the ratios. This explains the rather small α_s correction that we give in Eq. (6). For a thorough analysis, see [66,67].

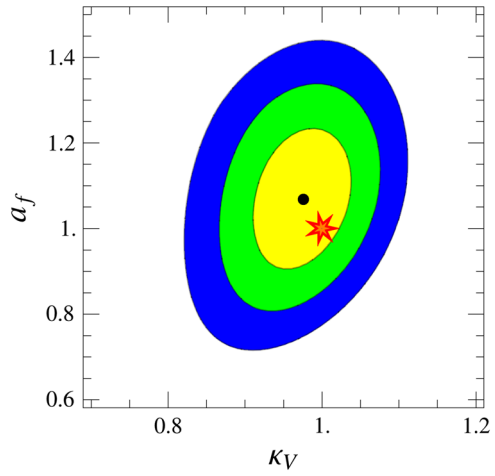

FIG. 1 (color online). Fit results for a_f vs κ_V. The black dot indicates the best-fit value. The yellow (white), green (medium grey), and blue (dark grey) areas represent the 68%, 95%, and 99.7% confidence-level regions, respectively. The red star shows the SM point $(\kappa_V, a_f) = (1, 1)$.

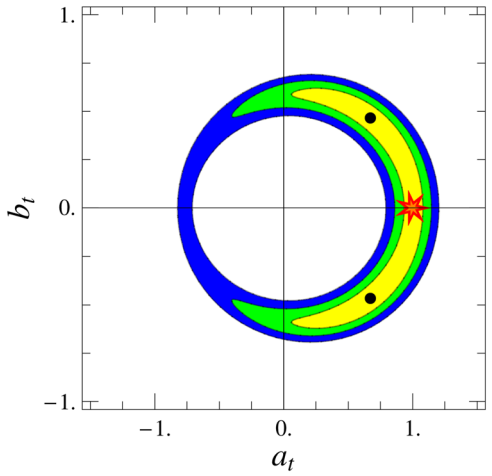

FIG. 2 (color online). Fit results for a_t vs b_t. Black dots indicate the best-fit values. The yellow (white), green (medium grey), and blue (dark grey) areas represent the 68%, 95%, and 99.7% confidence-level regions, respectively. The red star shows the SM point $(a_t, b_t) = (1, 0)$. The fit to a_t, b_t is performed while keeping all other parameters fixed to their SM values, i.e., $\kappa_V = 1$, $a_f = 1$, and $b_f = 0$ for any $f \neq t$.

for positive values of a_f and κ_V. An excess seen initially in the $h \to \gamma\gamma$ channel (excess which is now reduced in ATLAS Collaboration data and absent in CMS Collaboration data) pointed to negative values of a_f, which would have had serious consequences on unitarity [70,71]. In the figure, the black dot at (0.97, 1.06) indicates the best-fit value, while the yellow, green, and blue regions correspond to the 68%, 95%, and 99.7% confidence level regions, respectively. The SM value of $(\kappa_V, a_f) = (1, 1)$ is indicated by a red star. Analyses performed by CMS Collaboration [72] find a best-fit value at slightly smaller values of κ_V, while fits performed by ATLAS Collaboration [73] indicate larger values of κ_V. Since we have used both sets of data, we arrive at a middle point, in very good agreement with the SM expectation. We found good agreement with the fits of ATLAS and CMS Collabortions when we use only their respective data sets.

We next perform a fit to the parameters a_t and b_t—the CP-even and CP-odd Higgs-top quark couplings. All other parameters are fixed to their SM values, i.e., $\kappa_V = 1$, $a_f = 1$, and $b_f = 0$ for any $f \neq t$. The results of this fit are shown in Fig. 2. Similar analyses have also been performed in Refs. [35,36,74]. We find two best-fit values, $(a_t, b_t) = (0.67, 0.46)$ and $(a_t, b_t) = (0.67, -0.46)$, which are symmetric about the b_t axis as expected. Remarkably, significant departures from the SM expectation are still possible for the CP-odd coupling. The shape of the 68%, 95%, and 99.7% confidence level regions in Fig. 2 can be easily understood by looking at Eqs. (5) and (6). In $gg \to h$, the a_t and b_t coefficients enter quadratically, weighed by the loop functions A_t^a and A_t^b, respectively. Therefore, while $gg \to h$ production is useful to constrain the overall a_t^2 and b_t^2 magnitudes, alone it is unable to distinguish between scalar and pseudoscalar effects. Inclusion of the $h \to \gamma\gamma$ decay channel substantially improves the discriminating power. The important point is that, in this decay channel, the scalar-coupling contribution, contrary to the pseudoscalar one, interferes with the W contribution. In particular, for $a_t > 0$, as in the SM, this interference is destructive. On the other hand, for a_t negative, the branching ratio gets enhanced with respect to the SM one by both the scalar and the pseudoscalar contributions, thus making $\Gamma(h \to \gamma\gamma)$ too large. This is the reason why $a_t < 0$ is less favored than $a_t > 0$ in Fig. 2. Specifically, $a_t = 0$ does not fit the data either because, in this case, the W loop is too large and cannot obviously be compensated by the b_t contribution, irrespective of the value of b_t.

Next we look at the effect of the parameters κ_{gg}, $\kappa_{\gamma\gamma}$, $\tilde{\kappa}_{gg}$, and $\tilde{\kappa}_{\gamma\gamma}$, introduced in Eqs. (7). In particular, we would like to investigate their impact on the value of b_t. By inspection of Eqs. (7), it is clear that an arbitrary (common) value for $\tilde{\kappa}_{gg}$ and $\tilde{\kappa}_{\gamma\gamma}$ can always be compensated by b_t. Therefore, a simultaneous fit of Higgs-rate data to $\tilde{\kappa}_{gg}$, $\tilde{\kappa}_{\gamma\gamma}$, and b_t would result in the flat direction $|b_t| = -|\tilde{\kappa}_{gg}| = -|\tilde{\kappa}_{\gamma\gamma}|$, with $|b_t|$ arbitrary. We quote, as an example, a fit where we set $\tilde{\kappa}_{gg} = \tilde{\kappa}_{\gamma\gamma} = -1$ and $\kappa_{gg} = \kappa_{\gamma\gamma} = 0$. We find the best-fit point $(a_t = 0.67, b_t = 1.46)$ and that the various confidence level contours have shifted by $+1$ in the b_t direction, allowing for correspondingly larger values of b_t than the fit of Fig. 2. We would expect a second best-fit point at $(a_t = 0.67, b_t = 0.54)$, according to the discussion in the previous paragraph, and as displayed in Fig. 2. We actually find that the χ^2 value of this second solution is not exactly equal to the χ^2 at the best-fit point, although the relative difference is puny, 2×10^{-5}. Exact degeneracy is lifted by

the tagged $t\bar{t}h$ data in Table VI, to which the $\pm(b_t + \tilde{\kappa}_{gg,\gamma\gamma})$ symmetry does not apply, at variance with the rest of the data. This example demonstrates that $t\bar{t}h$ data would *in principle* be able to resolve the degeneracy in the b_t solutions, but their discriminating power is limited by their small statistical weight as compared with the rest of Higgs-rate data.

Altogether, this example is meant to show the inherent limitation of using indirect effects to probe the b_t interaction. As a matter of fact, in spite of using a very minimal set of parameters, data do not rule out a nonzero b_t. Furthermore, on introducing additional sources of pseudoscalar interactions, even larger values of b_t can be accommodated. Finally, since signal strengths are CP-even quantities (and therefore not linear in b_t), they do not provide information on the sign of b_t. All such ambiguities in the determination of a_t and b_t could only be resolved with more direct probes, as discussed in the remainder of this work.

III. ASSOCIATED PRODUCTION OF THE HIGGS BOSON WITH A $t\bar{t}$ PAIR

A. Kinematics of $t\bar{t}h$ production: scalar- vs pseudoscalar-Higgs boson cases

Of the four production modes (ggF, VBF, Vh, $t\bar{t}h$, with $V = W^{\pm}, Z$) of the Higgs bosons at the LHC, $t\bar{t}h$ production has the smallest cross section. Search strategies for the $t\bar{t}h$ process at the LHC have been studied in various Higgs decay modes [75,76]: $b\bar{b}$ [52,53], $\tau^+\tau^-$ [54], and W^+W^- [55–57]. The complicated final state of the process, with the top quark decaying to a bottom quark and a W boson, which in turn may decay either hadronically or leptonically, as well as the large backgrounds to the process make this a difficult channel to study at the LHC. Note, on the other hand, that $t\bar{t}h$ production can be studied very precisely at a future linear collider such as the ILC [77]. Sufficiently high rates for this process are possible at such colliders [78–84] and can therefore be used to extract CP information [85–93] by exploiting angular correlations and/or polarization of the top pair.

As noted in the previous section, studying $t\bar{t}h$ production at the LHC, though challenging, is a necessary undertaking; among the other reasons in order to unambiguously determine the parity of the Higgs coupling to the top quark, and to reveal potential CP-violating effects in the Higgs-top coupling. In this section, we wish to point out the major differences in the kinematics of the top and Higgs boson that a scalar vs a pseudoscalar Higgs boson entails for $t\bar{t}h$ production at the LHC. This has been discussed in the literature in quite some detail. See, for example, Refs. [87,94–100] and references therein for studies of the CP nature of the $t\bar{t}h$ vertex at the LHC. Many of these employ optimal observables [87,101] or the modern incarnation of the technique, the multivariate analysis. The aim of the present work at large, is to search for and explore *laboratory-frame observables* able to probe the nature of the $t\bar{t}h$ interactions at the LHC, in spite of the hadronic environment. Our analyses are performed on 14 TeV LHC collisions at the parton level, simulated thanks to the MadGraph package [102]. Events are simulated using the `CTEQ6L1` [103] parton distribution function with the pdf scale set by $\sqrt{\hat{s}}$. Note that in this section where we do not consider the decay of the Higgs boson or the top, we do not apply any selection cuts. In the next section, where we do consider the decay of the Higgs boson (to a pair of b quarks) and the leptonic decay of the top quarks, we impose cuts as follows:

(i) Transverse momentum: $p_{t_{\rm jet}} > 20\,{\rm GeV}$, $p_{t_{\rm lepton}} > 10\,{\rm GeV}$.
(ii) Pseudorapidity: $|\eta_{\rm jet}| < 5$, $|\eta_{b-{\rm jet}}| < 2.5$, $|\eta_{\rm lepton}| < 2.5$.
(iii) Separation between jets and leptons: $\Delta R_{lj} > 0.4$, $\Delta R_{jj} > 0.4$.

Next-to-leading order (NLO) QCD corrections have first been studied in [104–107]. These results have recently been confirmed by the use of automatic NLO tools including parton shower and hadronization [95,108–110]. More recently electroweak radiative corrections have also been studied [111,112]. In this first exploratory study, we do not consider the effect of NLO corrections, backgrounds, hadronization, initial and final state radiation, or detector effects. We will however briefly comment on effects such as parton shower and jet radiation for one of the important observables. A more detailed analysis will appear later.

As a first step, let us try to understand the kinematics of $t\bar{t}h$ production without considering the decays of the Higgs boson or the $t\bar{t}$ quarks. The relevant Feynman diagrams are shown in Fig. 3. We have grouped the diagrams into three categories: quark-initiated, gluon-initiated s channel, and gluon-initiated t channel. Diagrams where the production is

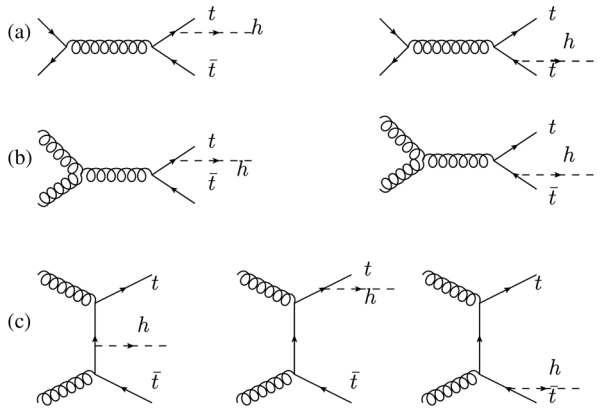

FIG. 3. Feynman diagrams for Higgs production in association with a $t\bar{t}$ pair at the LHC. Diagrams where the production is mediated by a Z boson or a photon have been omitted. Three more diagrams can be realized by exchanging the two gluon lines in the last row labeled (c). (a) Quark initiated, (b) gluon initiated s-channel, and (c) gluon initiated t-channel.

mediated by a Z boson or a photon have been omitted. Three more diagrams can be realized by exchanging the two gluon lines in the last row labeled (c).

The first distribution we consider is the production cross section near threshold. It has been pointed out that the threshold behavior of the cross section for a scalar *vs* a pseudoscalar Higgs boson is very different at an e^+e^- collider [88–90]. More specifically, the *rate* of increase of the cross section with the center of mass energy of the collision is suppressed in the case of the pseudoscalar Higgs coupling by a factor of ρ, where $\rho=(\sqrt{s}-2m_t-m_h)/\sqrt{s}$ parametrizes the proximity to the production threshold. This factor can be easily understood from arguments of parity and angular-momentum conservation [88]. Close to the energy threshold, the simultaneous demand of angular momentum and parity conservation implies that for a scalar the total angular momentum of the $t\bar{t}h$ system will be zero, while for a pseudoscalar, it will be one. Since the process is mediated through s-channel production, the pseudoscalar production will be suppressed near threshold. Note that the total cross section and not just the behavior near the threshold is different for a scalar and a pseudoscalar for the same Yukawa coupling strength.

At the LHC, several competing production mechanisms are at work, and it is nontrivial that a similar difference in the threshold rise be also visible. Indeed the same behavior as in the e^+e^- case is observed in the quark-initiated process of pp collisions, which is a spin-1, s-channel process, but this contribution is negligible at the LHC. The dominant gg-initiated process, has contributions from both s-channel and t-channel diagrams as shown in Fig. 3. While for pseudoscalar production, the s channel displays a similar suppression by ρ near threshold, the t channel does not. We find however that the cross section near the production threshold in the t channel displays a suppression by a factor proportional to $(m_h/m_t)^4$. As a result, the production cross section near threshold does show interesting behavior.

In the left panel of Fig. 4, we show the normalized invariant mass distributions of the $t\bar{t}h$ system for the pseudoscalar $(a_t=0,b_t=1)$, the scalar $(a_t=1,b_t=0)$ case, and the CP-violating case.

We see that the rate of increase of the cross section with the invariant mass of the $t\bar{t}h$ system is much more rapid for the scalar than for the pseudoscalar case. This is an important distinguishing feature and could be used to probe the nature of the Higgs-top quark coupling. The right panel of Fig. 4 shows the same distributions, but normalized to the total cross section (i.e., $d\sigma/dM_{t\bar{t}h}$). We observe, as expected, that for the same coupling magnitude, the cross section for the pseudoscalar case is suppressed with respect to the scalar case. It is important to investigate how this discriminating feature remains once NLO corrections and additional radiation [95,104–110] are included. To address this issue, we have checked that, at LO, parton showering (PS) and radiation effects have a minimal effect on this observable. We have checked, using up to two additional jets in the matching scheme defined in [113], that there is no noticeable change in the $M_{t\bar{t}h}$ distributions. This is an encouraging result before a simulation including NLO and PS is implemented.

While the invariant mass distribution is a useful observable to probe the nature of the Higgs-top couplings, its measurement is not straightforward. In fact, it requires complete knowledge of the top and Higgs momenta, whose reconstruction is challenged by uncertainties on jet energies and, in particular, by missing energy, in decay channels including neutrinos.

We note incidentally that, rather than trying to extract the full distribution itself, it might be easier to consider ratios of cross sections in two $M_{t\bar{t}h}$ intervals.

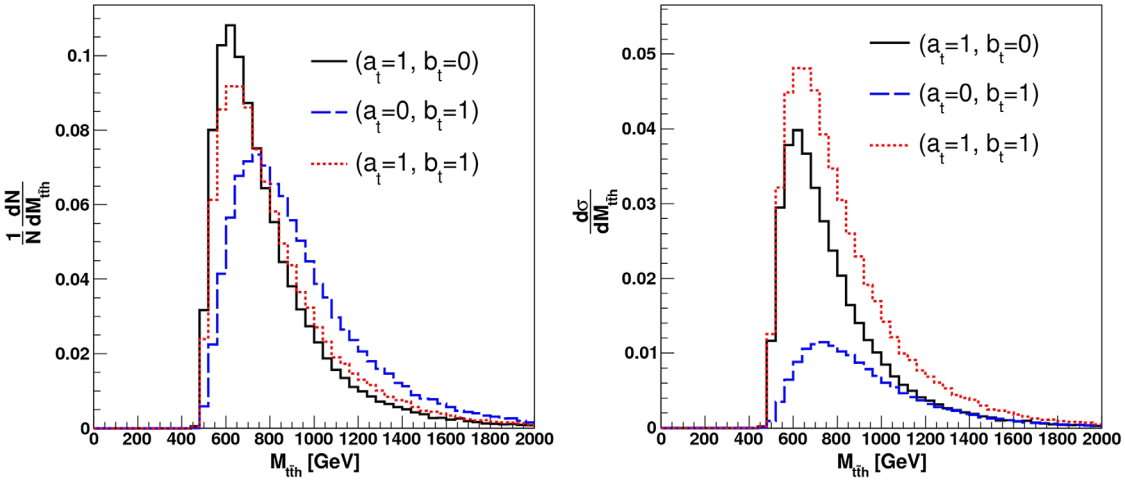

FIG. 4 (color online). *(Left panel)* The invariant-mass distribution of the $t\bar{t}h$ system, normalized to unity. *(Right panel)* The differential cross section with respect to the $t\bar{t}h$ invariant mass. In either panel, the SM distribution $(a_t=1,b_t=0)$ is shown with a solid black line, the pseudoscalar case $(a_t=0,b_t=1)$ with a blue dashed line, and the CP-violating case $(a_t=1,b_t=1)$ with a dotted red line.

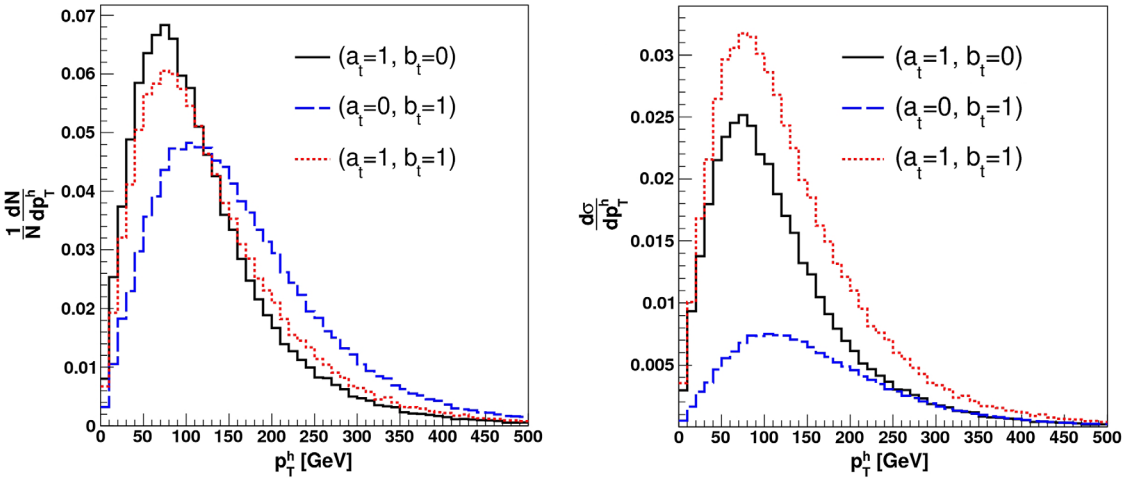

FIG. 5 (color online). *(Left panel)* The distribution of the transverse momentum of the Higgs boson (p_T^h), normalized to unity. *(Right panel)* The differential cross section with respect to the transverse momentum of the Higgs boson (p_T^h). In either panel, the SM distribution ($a_t = 1, b_t = 0$) is shown with a solid black line, the pseudoscalar case ($a_t = 0, b_t = 1$) with a blue dashed line, and the *CP* violating case ($a_t = 1, b_t = 1$) with a dotted red line.

The complications mentioned above motivate us to look for alternatives to the invariant-mass distribution $M_{t\bar{t}h}$. One first possibility, that has also been considered in Refs. [94,95], is the transverse momentum of the Higgs boson. Its distributions are shown in Fig. 5, with normalizations analogous to Fig. 4. As a general feature, we note that the transverse momentum of the Higgs boson (p_T^h) displays a behavior akin to the invariant-mass distribution $M_{t\bar{t}h}$. Noteworthy is the fact that p_T^h is pushed to larger values in the pseudoscalar case ($a_t = 0, b_t = 1$) in comparison to the SM distribution ($a_t = 1, b_t = 0$).

The larger transverse momentum of the Higgs boson in the pseudoscalar case will have an effect on an observable that can be measured quite easily, namely, the azimuthal-angle separation between the top quark and antiquark, $\Delta\phi(t, \bar{t})$. In order to measure this quantity, one needs only to reconstruct one of the top momenta at most. The distribution for this observable is shown in Fig. 6 for the SM ($a_t = 1, b_t = 0$), the pseudoscalar ($a_t = 0, b_t = 1$), and the *CP*-violating case ($a_t = 1, b_t = 1$). We see that in either case $\Delta\phi(t, \bar{t})$ peaks at large values $\pm\pi$. However, for the pseudoscalar case, the distribution is more flat in comparison to the SM. This can be understood as follows. For events produced near the energy threshold, the transverse momentum of the Higgs boson is small. This means that the top pair will be produced mostly back to back. This accounts for the peaks observed at $|\Delta\phi(t, \bar{t})| = \pi$. Because the p_T^h distribution in the pseudoscalar case is pushed to larger values, this will give rise to a flatter distribution in $\Delta\phi(t, \bar{t})$. Considering that the construction of this observable only requires information about the direction of the various decay products, it can be readily used in both the hadronic as well as semileptonic decay modes of the top quarks. Uncertainties in the measurement of this observable are likely to be much reduced in comparison to $M_{t\bar{t}h}$.

One may also attempt to address the question, which of the observables, $M_{t\bar{t}h}$, p_T^h or $\Delta\phi(t, \bar{t})$, better discriminates between scalar and pseudoscalar production, although at the experimental level, one may rather opt for reconstructing all three and use them in a multivariate analysis. To answer this question, we perform a likelihood analysis, akin to the one described in Ref. [28]. For the sake of comparison, we assume 100% efficiency in the construction of both observables, neglect backgrounds and normalize the total cross section for scalar and pseudoscalar production to be the same. As a result, the luminosities

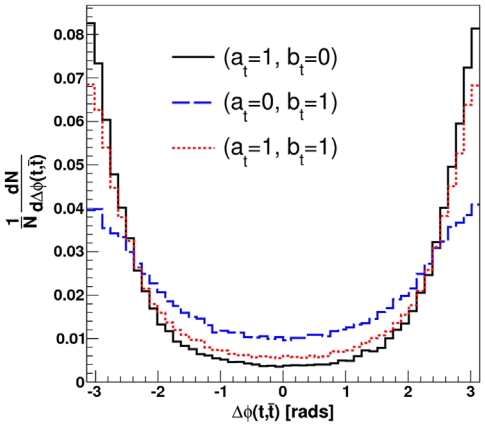

FIG. 6 (color online). The distribution of the azimuthal-angle difference between the top pair [$\Delta\phi(t, \bar{t})$], normalized to unity. The SM distribution ($a_t = 1, b_t = 0$) is shown with a solid black line, the pseudoscalar case ($a_t = 0, b_t = 1$) with a blue dashed line, and the *CP*-violating case ($a_t = 1, b_t = 1$) with a dotted red line.

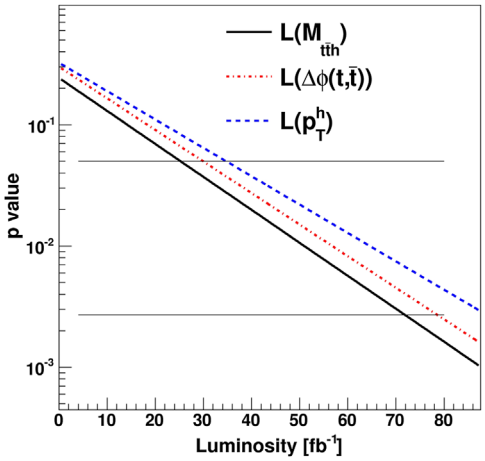

FIG. 7 (color online). p value as a function of the integrated luminosity for the distinction between the SM ($a_t = 1, b_t = 0$) and the pseudoscalar case ($a_t = 0, b_t = 1$) using likelihoods constructed from the observables $M_{t\bar{t}h}$ (black solid line), p_T^h (blue dashed line), and $\Delta\phi(t,\bar{t})$ (red dot-dashed line). We only include statistical uncertainties associated to the $t\bar{t}h$ signal, in the absence of backgrounds. The two horizontal lines indicate the 2σ (top line) and 3σ (bottom line) exclusion limits.

that one will achieve from such an analysis are not realistic and are only to be used to appreciate the discriminating power of the two observables. We use histograms of the distributions binned with 20 intervals in the range (0,2000) GeV, (0,500) GeV, and $(-\pi, \pi)$ for $M_{t\bar{t}h}$, p_T^h and $\Delta\phi(t,\bar{t})$, respectively.

In Fig. 7, we show the variation of the p value for the pseudoscalar hypothesis measured from the median value of the SM (null) hypothesis. We have used three likelihood functions, $L(M_{t\bar{t}h})$, $L(p_T^h)$, and $L(\Delta\phi(t,\bar{t}))$. We reiterate that the absolute values of the luminosities in this figure are not to be taken seriously, as we are only interested in the slopes of the lines. From this figure, we can infer that the $M_{t\bar{t}h}$ distribution has a slightly better discriminating power followed by $\Delta\phi(t,\bar{t})$ and then by p_T^h. However, the difference between the three likelihoods is very small. Since $\Delta\phi(t,\bar{t})$ and p_T^h will have better reconstruction efficiencies and reduced uncertainties in comparison to $M_{t\bar{t}h}$, the former are expected to perform much better in a more realistic analysis. We conclude that $\Delta\phi(t,\bar{t})$ and p_T^h are better suited observables to distinguish between a scalar and a pseudoscalar hypothesis.

So far we have only considered the kinematics of $t\bar{t}h$ production, without any regards to the decays of the top quarks or the Higgs boson. Furthermore, the observables we have constructed are not directly sensitive to CP-violating effects. We will address these issues in the next section.

It is interesting to note that, although a specific measurement of the $t\bar{t}h$ cross section cannot discriminate between a scalar and a pseudoscalar Higgs boson, the fact that the distributions are sensitive to its CP assignment means that by comparing a subset of the same cross section, one could in principle lift the degeneracy. Normalized to the SM cross section the inclusive $t\bar{t}h$ cross section at 14 TeV can be written as

$$\sigma/\sigma^{\rm SM} \simeq a_t^2 + 0.42 b_t^2. \tag{10}$$

A cut $\chi_{\rm cut}$, such as $p_T^h > 100$ GeV, increases the relative weight of the pseudoscalar contribution

$$\sigma(\chi_{\rm cut})/\sigma^{\rm SM}(\chi_{\rm cut})/ = a_t^2 + 0.60 b_t^2. \tag{11}$$

If both these measurements, Eqs. (10) *and* (11), were precise enough, combining them could return nonzero values for *both* a_t and b_t. While none of these cross sections is a measure of CP violation, the combination of both cross sections may lead nonzero values for both a_t and b_t, which is an indirect measure of CP violation. At the lower center of mass energy of 8 TeV, the inclusive cross section benefits less the pseudoscalar contribution. In fact, even at 14 TeV, the pseudoscalar contribution is enhanced relative to the scalar contribution in the more energetic regions of phase space. The cross section at 8 TeV center of mass is parametrized as

$$\sigma_{8\ \rm TeV}/\sigma_{8\ \rm TeV}^{\rm SM} \simeq a_t^2 + 0.31 b_t^2. \tag{12}$$

It should be remembered at this point that precision of cross section ratios as probes of BSM physics is to some extent limited by QCD uncertainties in the cross section predictions [114].

B. Spin correlations in $t\bar{t}$ decay products

The nature of the Higgs-top coupling in Eq. (1) also affects spin correlations between the top and the antitop quarks. The latter can be tested, for example, through azimuthal-angle differences between the momenta of the particles involved in the process [115–117]. We show in Fig. 8 the normalized distributions of $\Delta\phi(t,\bar{t})$ in unpolarized production for two helicity combinations of the final-state top quarks produced in association with a scalar or a pseudoscalar Higgs boson. The two helicity combinations we consider are like-helicity $(t_L\bar{t}_L + t_R\bar{t}_R)$ and unlike-helicity $(t_L\bar{t}_R + t_R\bar{t}_L)$ top pairs, in the laboratory frame. The conventions for helicity states and spinors are the same as in Ref. [118]. The figure shows that the scalar and, especially, the pseudoscalar cases produce different effects for different helicity combinations. The most striking difference occurs between the unlike-helicity combination for pseudoscalar production, which yields a flat distribution, and the remaining distributions, all clearly peaked at $|\Delta\phi(t,\bar{t})| = \pi$.

A measure of the spin correlations can be defined through the following spin-correlation asymmetry in the laboratory frame

$$\zeta_{\rm lab} = \frac{\sigma(pp \to t_L\bar{t}_L h) + \sigma(pp \to t_R\bar{t}_R h) - \sigma(pp \to t_L\bar{t}_R h) - \sigma(pp \to t_R\bar{t}_L h)}{\sigma(pp \to t_L\bar{t}_L h) + \sigma(pp \to t_R\bar{t}_R h) + \sigma(pp \to t_L\bar{t}_R h) + \sigma(pp \to t_R\bar{t}_L h)}. \tag{13}$$

We find the following numerical values for the spin-correlation asymmetry for the different parity admixtures: $\zeta_{\rm lab}(a_t = 1, b_t = 0) = 0.22$, $\zeta_{\rm lab}(a_t = 0, b_t = 1) = 0.46$, and $\zeta_{\rm lab}(a_t = 1, b_t = 1) = 0.29$. These results can be combined in the following parametric formula

$$\zeta_{\rm lab} \simeq \frac{0.22a_t^2 + 0.19b_t^2}{a_t^2 + 0.42b_t^2} \tag{14}$$

valid for the case of the LHC at 14 TeV. The a_t, b_t dependence of $\zeta_{\rm lab}$ confirms our initial remark on the nature of the Higgs coupling affecting spin correlations. To be noted are the following points: (i) among the cases considered, the SM predicts the smallest value for $\zeta_{\rm lab}$; (ii) although the *CP*-violating case has a larger value for this coefficient, it is only marginally higher than the SM. This is due to the scalar cross sections being larger than the pseudoscalar ones; (iii) the asymmetry in Eq. (13) is not sensitive to *CP*-violating effects as it is a *CP*-even quantity. The same is also true for the observables described in the previous section. Note however that a measurement of a_t and b_t is nonetheless an indirect measure of *CP* violation. Theoretically, a value for ζ which deviates from 0.22 or 0.46, corresponds to both a_t and b_t being nonzero.

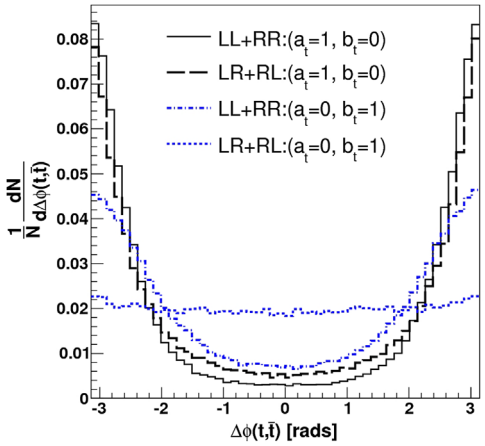

FIG. 8 (color online). Distributions of the azimuthal-angle difference between the top pair, $\Delta\phi(t, \bar{t})$, normalized to unity. The four histograms refer to $t\bar{t}h$ production with like-helicity top pairs ($t_L\bar{t}_L + t_R\bar{t}_R$) and a scalar (black solid line) or a pseudoscalar (blue dash-dotted line) Higgs boson, as well as to $t\bar{t}h$ production with unlike-helicity top pairs ($t_L\bar{t}_R + t_R\bar{t}_L$) and a scalar (black dashed line) or a pseudoscalar (blue dotted line) Higgs boson, in the laboratory frame.

While the spin-correlation asymmetry in Eq. (13) may serve as a yardstick for the order of magnitude of the effects to be expected, it is not an easily measurable quantity at the LHC. Spin-correlation observables typically exploit the fact that the $t\bar{t}$ spin information is passed on to the kinematic distributions of the decay products of the top quarks. In addition, the kinematics of the decay products are more likely to be affected by *CP* violation in the production process than the kinematics of the top quarks themselves, i.e., observables constructed using the decay products are more likely to be linearly sensitive to b_t.[5]

Let us first consider the dileptonic decay mode[6] of the top pair.[7] Note that in order to consider spin-correlation effects, we use the full matrix element for the process with a pair of leptons, neutrinos, b quarks, and the Higgs boson in the final state. The Breit-Wigner approximation is used for on shell top quarks. It is well-known that the azimuthal-angle difference between the antilepton and the lepton from the decay of t and $\bar{t}$, respectively, provides a good probe of spin-correlation effects in $t\bar{t}$ production [117,119–122], even in the laboratory frame. Furthermore, as the lepton angular distribution in the decay of the top is not affected by any nonstandard effects in the decay vertex, it is a pure probe of physics associated with the production process [117,123]. For $t\bar{t}h$ production, the t and $\bar{t}$ are not produced back to back (in the xy plane) since the Higgs momentum adds an extra degree of freedom to the system. As a result, spin-correlation effects in the azimuthal-angle difference will be washed out. It is possible to consider the angles between the two leptons in a different reference frame, where the kinematics of the $t\bar{t}h$ system does not dissolve the effect of spin correlations. Distributions for such observables can be found in [40,94,124–126]. In Fig. 9, we show the distribution of one such angle, $\Delta\phi^{t\bar{t}}(\ell^+, \ell^-)$ [94,124,126]. $\Delta\phi^{t\bar{t}}(\ell^+, \ell^-)$ is defined as the difference between the azimuthal angle of the ℓ^+ momentum in the rest frame of the top and the azimuthal angle of the ℓ^-

[5]In fact, *CP*-violating interference terms are more likely to be generated in the matrix element squared when we sum over helicities of the decay products since the matrix elements for production and decay can be linked through a density matrix.

[6]The observables that we will consider can be altered in an obvious way so that they can be used in the semileptonic or even hadronic decays.

[7]For the dileptonic channel, we apply the following set of cuts: p_T of jets > 20 GeV, $|\eta|$ of jets < 5, $|\eta|$ of b jets < 2.5; p_T of leptons > 10 GeV, $|\eta|$ of leptons < 2.5. $\Delta R_{lj} > 0.4$, $\Delta R_{jj} > 0.4$.

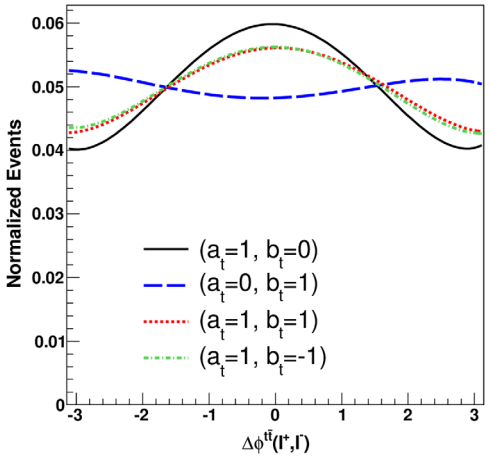

FIG. 9 (color online). Normalized distributions for $\Delta\phi^{t\bar{t}}(\ell^+,\ell^-)$ in $t\bar{t}h$ production. Distributions are shown for the SM $(a_t=1,b_t=0)$ (black solid line), for the pseudoscalar case $(a_t=0,b_t=1)$ (blue dashed line), and for two CP-violating cases, $(a_t=1,b_t=1)$ (red dotted line) and $(a_t=1,b_t=-1)$ (green dot-dashed line).

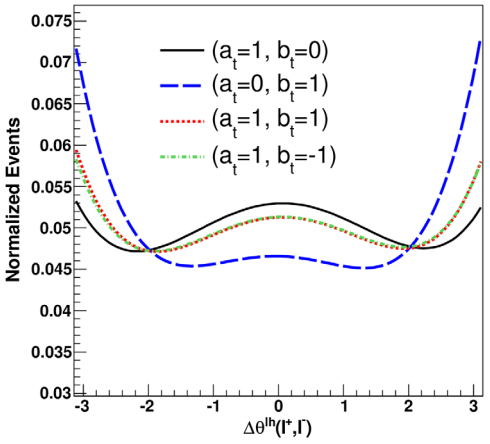

FIG. 10 (color online). Normalized distributions for $\Delta\theta^{\ell h}(\ell^+,\ell^-)$ in $t\bar{t}h$ production. Distributions are shown for SM $(a_t=1,b_t=0)$ (black solid line), for a pseudoscalar $(a_t=0,b_t=1)$ (blue dashed line), and for two CP violating cases, $(a_t=1,b_t=1)$ (red dotted line) and $(a_t=1,b_t=-1)$ (green dot-dashed line).

momentum evaluated in the rest frame of the antitop [124,126].[8]

From the figure, we can see that the SM $(a_t=1,b_t=0)$ distribution peaks at $\Delta\phi^{t\bar{t}}(\ell^+,\ell^-)=0$, while the pseudoscalar $(a_t=0,b_t=1)$ case has a minimum at $\Delta\phi^{t\bar{t}}(\ell^+,\ell^-)=0$. We have also considered two CP-violating cases, $(a_t=1,b_t=1)$ and $(a_t=1,b_t=-1)$, which show a behavior qualitatively similar to the SM case. Furthermore, since the distributions for the two CP-violating cases appear to be the same, we can conclude that the two observables do not depend on b_t linearly and hence do not probe CP violation in the production process in a direct manner.

Although the $\Delta\phi^{t\bar{t}}(\ell^+,\ell^-)$ and other observables considered in the literature [40] do manage to differentiate between a scalar and a pseudoscalar, they are extremely difficult to construct at the LHC, especially because a full reconstruction of all momenta of the $t\bar{t}h$ system is necessary. In addition, the uncertainties in the measurement of the various momenta involved will carry over to the uncertainties in the measurement of these observables as we transform between different frames of reference. We therefore explore the option of constructing laboratory-frame observables. One such observable is $\Delta\theta^{\ell h}(\ell^+,\ell^-)$, defined as the angle between the two lepton momenta projected onto the plane perpendicular to the h direction in the laboratory frame:

$$\cos(\Delta\theta^{\ell h}(\ell^+,\ell^-))=\frac{(\vec{p}_h\times\vec{p}_{\ell^+})\cdot(\vec{p}_h\times\vec{p}_{\ell^-})}{|\vec{p}_h\times\vec{p}_{\ell^+}||\vec{p}_h\times\vec{p}_{\ell^-}|}. \quad (16)$$

This definition can be understood from the following argument. Recall that, for two-body $t\bar{t}$ production, the azimuthal angle of the two leptons is sensitive to spin correlation effects. The $t\bar{t}h$ system follows three body kinematics, hence the $t\bar{t}$ can be understood to "recoil" off the Higgs boson. It follows that, when we project the two lepton momenta onto the plane perpendicular to the Higgs direction, the angle between them will also be sensitive to such spin-correlation effects.

The distribution for $\Delta\theta^{\ell h}(\ell^+,\ell^-)$ is shown in Fig. 10. From this plot we see that, similarly as for the angles considered before, there is an extremum at $\Delta\theta^{\ell h}(\ell^+,\ell^-)=0$ for all cases considered. The SM distribution displays a pronounced peak at $\Delta\theta^{\ell h}(\ell^+,\ell^-)=0$, while the pseudoscalar distribution is smaller and flatter in the whole region $[-\pi/2,+\pi/2]$, whereas it is larger at $|\Delta\theta^{\ell h}(\ell^+,\ell^-)|=\pi$. Hence, this observable can be used to probe the CP nature of the $t\bar{t}h$ interaction. On the other hand, being by its definition a CP-even observable, $\Delta\theta^{\ell h}(\ell^+,\ell^-)$ does not distinguish between the two CP-violating cases $(a_t=1,b_t=1)$ and $(a_t=1,b_t=-1)$, that in fact have exactly the same behavior in Fig. 10. In this respect, it is worth noting explicitly that, while the plot in Fig. 10 spans the range $[-\pi,\pi]$, $\Delta\theta^{\ell h}(\ell^+,\ell^-)$ is, according to Eq. (16), defined

[8]In constructing the $\ell^\pm$ momenta as described, we keep fixed for all events the choice of the x and y axes, and the z axis is chosen, as customary, to lie along the beam direction. While individually the azimuthal angles for the ℓ^+ and ℓ^- momenta do depend on the choice of the x and y axes, their difference, as in $\Delta\phi$, does not. $\Delta\phi$ depends only on the choice of the beam axis. In fact, one can construct $\Delta\phi$ from the following formula

$$\cos(\Delta\phi^{t\bar{t}}(\ell^+,\ell^-))=\frac{(\hat{z}\times\vec{p}^{\,\bar{t}}_{\ell^-})\cdot(\hat{z}\times\vec{p}^{\,t}_{\ell^+})}{|\vec{p}^{\,\bar{t}}_{\ell^-}||\vec{p}^{\,t}_{\ell^+}|}, \quad (15)$$

that shows dependence only on the $\hat{z}$ direction. In this formula, the superscripts t ($\bar{t}$) indicate that the given momentum is calculated in the rest frame of the t ($\bar{t}$).

only in the interval $[0,\pi]$. In order to assign a given event to the $[0,\pi]$ or to the $[-\pi,0]$ interval, one needs an observable proportional to $\sin\Delta\theta^{\ell h}(\ell^+,\ell^-)$, for example, $\mathrm{sgn}(\vec{p}_h\cdot(\vec{p}_{\ell^+}\times\vec{p}_{\ell^-}))$, where "sgn" indicates that we consider the sign of the term in brackets.

We conclude this section by noting that, albeit not explicitly shown here, other distributions that, like the one in Fig. 10, are also able to distinguish the different vertex structures, would arise if we were to replace one or both of the lepton momenta in Eq. (16) by W-boson momenta. Such distributions are useful in semileptonic or fully hadronic decays of the top pair.

C. *CP*-violating observables

So far we have confined ourselves to observables that are not sensitive to CP-violating effects. An observable sensitive to CP violation must be odd under CP transformations. Such quantities have been considered in the context of e^+e^- colliders [86,90,117,123], and these results were exploited in the optimal-observable analysis of Ref. [87]. More recently, in the context of the LHC, a CP-odd observable was proposed in Ref. [40] as follows

$$\alpha \equiv \mathrm{sgn}(\vec{p}_t^{\,t\bar{t}}\cdot(\vec{p}_{\ell^-}^{\,t\bar{t}}\times\vec{p}_{\ell^+}^{\,t\bar{t}})). \tag{17}$$

Here the superscripts indicate that the corresponding momenta are constructed in the center-of-mass frame of the $t\bar{t}$ system. Because of "sgn", α can only take values of ±1.

Although this observable is sensitive to CP violation linear in b_t, it suffers from the same problem as before: it is very difficult to reconstruct at the LHC as all momenta of the $t\bar{t}h$ system need to be determined. We suggest an alternative CP-odd observable that can be constructed *entirely* out of laboratory-frame quantities:

$$\beta \equiv \mathrm{sgn}((\vec{p}_b-\vec{p}_{\bar{b}})\cdot(\vec{p}_{\ell^-}\times\vec{p}_{\ell^+})). \tag{18}$$

Note that, in order to correctly identify jets originating from a b and $\bar{b}$ quark, one needs not reconstruct the top or antitop momenta, of course. Various algorithms can be used to differentiate b from $\bar{b}$ jets.[9]

The distribution obtained when we multiply β by $\Delta\theta^{\ell h}(\ell^+,\ell^-)$ is shown in Fig. 11. This distribution displays an asymmetry for the two CP-violating cases. Specifically, the distribution for $(a_t=1,b_t=1)$ yields larger values in the positive x axis, whereas the distribution for $(a_t=1,b_t=-1)$ is larger on the negative x axis.

We thus have a quantity that not only is sensitive to CP violation but is constructed entirely out of laboratory-frame kinematics. In addition, a measurement of this observable demands only reconstruction of the Higgs momentum, whereas reconstruction of the top pair momenta is not necessary. Note on the other hand that this observable cannot be generalized easily to the case of semileptonic or hadronic decays of the top since it is not possible to differentiate between the quark and antiquark jet originating from W-boson decays.

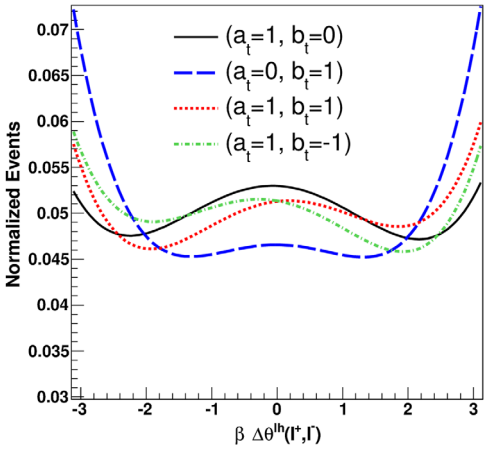

FIG. 11 (color online). Normalized distributions for $\beta\cdot\Delta\theta^{\ell h}(\ell^+,\ell^-)$ in $t\bar{t}h$ production. Distributions are shown for the SM $(a_t=1,b_t=0)$ (black solid line), for the pseudoscalar case $(a_t=0,b_t=1)$ (blue dashed line), and for two CP-violating cases, $(a_t=1,b_t=1)$ (red dotted line) and $(a_t=1,b_t=-1)$ (green dot-dashed line).

It is useful to define CP asymmetries with the observables $\alpha\times\Delta\theta^{t\bar{t}}(\ell^+,\ell^-)$ [40] and $\beta\times\Delta\theta^{\ell h}(\ell^-,\ell^+)$ as follows

$$A_{t\bar{t}}=\frac{\sigma(\alpha\times\Delta\theta^{t\bar{t}}(\ell^+,\ell^-)>0)-\sigma(\alpha\times\Delta\theta^{t\bar{t}}(\ell^+,\ell^-)<0)}{\sigma(\alpha\times\Delta\theta^{t\bar{t}}(\ell^+,\ell^-)>0)+\sigma(\alpha\times\Delta\theta^{t\bar{t}}(\ell^+,\ell^-)<0)} \tag{19}$$

and

$$A_{\mathrm{lab}}=\frac{\sigma(\beta\times\Delta\theta^{\ell h}(\ell^-,\ell^+)>0)-\sigma(\beta\times\Delta\theta^{\ell h}(\ell^-,\ell^+)<0)}{\sigma(\beta\times\Delta\theta^{\ell h}(\ell^-,\ell^+)>0)+\sigma(\beta\times\Delta\theta^{\ell h}(\ell^-,\ell^+)<0)}. \tag{20}$$

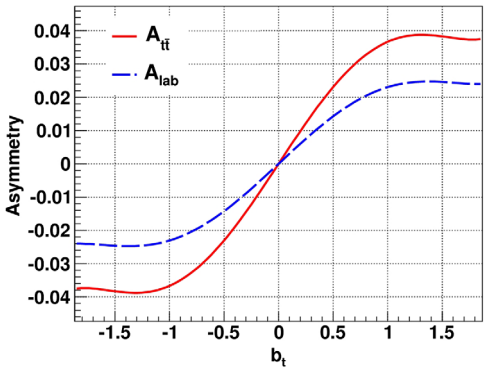

FIG. 12 (color online). Dependence of the asymmetries $A_{t\bar{t}}$ (red solid line) and A_{lab} (blue dashed line) on the strength of the CP-odd component b_t. In this plot, a_t is kept fixed to unity.

[9]See, for example, Refs. [127–130] and references therein.

The dependence of these asymmetries on b_t (keeping $a_t = 1$ fixed) is shown in Fig. 12. We observe that both asymmetries are sensitive to the sign of b_t (and hence linear in b_t), being negative for negative values of b_t and positive for positive values of this parameter. The magnitude of the asymmetry $A_{t\bar{t}}$ is larger than the magnitude of $A_{\rm lab}$ for a given value of b_t. However, we emphasize again that $A_{\rm lab}$ is constructed out of laboratory-frame quantities only and as such it is expected to be more easily measurable and to have less systematic uncertainties than $A_{t\bar{t}}$.

IV. CONCLUSIONS

We have considered a Higgs-top Yukawa coupling that allows for a general scalar and pseudoscalar Higgs admixture, and have explored the possibility to probe this coupling in a model-independent framework. We find that, although constraining, the information provided by the Higgs rates, or by low-energy observables such as EDMs, does not suffice to provide conclusive evidence about the nature of this coupling. The arguably best way of probing this coupling unambiguously is its direct measurement. While certainly challenging in a hadronic environment like the LHC's, a measurement of this coupling would provide crucial information on the properties of the scalar coupled to the SM's heaviest particle, let alone the possibility of unveiling *CP*-violating effects.

We have investigated some of the possible kinematic observables that could be used to discriminate a scalar from a pseudoscalar-like coupling at the LHC, focusing on the possibility of quantities constructed out of just *laboratory-frame* kinematics. The information about the nature of the coupling is carried by the threshold behavior of the total invariant mass of the $t\bar{t}h$ system, which is however very difficult to reconstruct. We find that similar information is encoded in the distributions of two experimentally simpler quantities, namely, the transverse momentum of the Higgs boson and the azimuthal-angle separation between the $t\bar{t}$ pair.

We furthermore exploit the fact that the information about the nature of the $t\bar{t}h$ interaction is also passed on to the decay products of the $t\bar{t}$ pair. Spin correlations between the t and the $\bar{t}$ are likewise affected by the scalar vs pseudoscalar nature of this interaction. We suggest several *laboratory-frame* observables that are affected by the spin correlations and hence can be used to probe the Higgs-top interactions in all possible decay modes of the $t\bar{t}$ pair: dileptonic, semileptonic, and hadronic.

Finally, in the dilepton channel, we construct an observable that bears linear dependence on b_t and hence is sensitive to *CP*-violating effects. We determine the corresponding *CP* asymmetry and show how it is sensitive to both the strength and the sign of b_t.

It goes without saying that, being an exploratory study aimed at the definition of laboratory-frame observables, the analysis performed here is simplistic. In particular, it is a leading-order and parton-level analysis. While refinements towards a more realistic analysis (like inclusion of NLO, detector smearing, hadronization effects, etc.) will change quantitatively several of our distributions, they are not expected to modify our main conclusions. More detailed investigations are in progress.

ACKNOWLEDGMENTS

The authors acknowledge hospitality of the Centre de Physique des Houches, where this work started in connection with the workshop PhysTeV 2013. We also thank Gustaaf Broijmaans for raising very useful questions. KM acknowledges the support of the Rhône-Alpes CMIRA programme and the excellence cluster Labex ENIGMASS as well as support by the National Science Foundation under Grant No. PHY-0854889. R. M. G. wishes to acknowledge support from the Department of Science and Technology, India under Grant No. SR/S2/JCB-64/2007 under the J. C. Bose Fellowship scheme. R. M. G. also wishes to acknowledge support from the French ANR

TABLE I. Data on signal strengths of $h \to \gamma\gamma$ recorded by ATLAS and CMS Collaborations, and at the Tevatron The percentages of each production mode in each data are given.

			Production mode			
Channel	Signal strength μ	m_h (GeV)	ggF	VBF	Vh	tth
ATLAS (4.5 fb^{-1} at 7 TeV + 20.3 fb^{-1} at 8 TeV) [131]						
Inclusive	1.17 ± 0.23	125.4	87.5%	7.1%	4.9%	0.5%
CMS (5.1 fb^{-1} at 7 TeV + 19.7 fb^{-1} at 8 TeV) [132]						
Inclusive	$1.14^{+0.26}_{-0.23}$	124.7	87.5%	7.1%	4.9%	0.5%
Tevatron (10.0 fb^{-1} at 1.96 TeV) [133]						
Combined	$6.14^{+3.25}_{-3.19}$	125	78%	5%	17%	0%

TABLE II. Data on signal strengths of $h \to Z^{(*)}Z^{(*)}$ recorded by ATLAS and CMS Collaborations. The percentages of each production mode in each data are given.

			Production mode			
Channel	Signal strength μ	m_h (GeV)	ggF	VBF	Vh	tth
ATLAS (4.8 fb^{-1} at 7 TeV + 20.7 fb^{-1} at 8 TeV) [134,135]						
Inclusive	$1.66^{+0.45}_{-0.38}$	124.51	87.5%	7.1%	4.9%	0.5%
CMS (5.1 fb^{-1} at 7 TeV + 19.6 fb^{-1} at 8 TeV) [6]						
Inclusive	$0.93^{+0.29}_{-0.25}$	125.6	87.5%	7.1%	4.9%	0.5%

TABLE III. Data on signal strengths of $h \to W^{(*)}W^{(*)}$ recorded by ATLAS Collaboration, CMS Collaboration, and Tevatron. The percentages of each production mode in each data are given.

			Production mode			
Channel	Signal strength μ	m_h (GeV)	ggF	VBF	Vh	tth
ATLAS (25 fb^{-1} integrated luminosity at 7 and 8 TeV) [136]						
ggF	$1.01^{+0.27}_{-0.25}$	125.36	100.0%	0%	0%	0%
VBF	$1.28^{+0.53}_{-0.45}$	125.36	0%	100%	0%	0%
CMS (up to 4.9 fb^{-1} at 7 TeV + 19.4 fb^{-1} at 8 TeV) [15]						
0/1 jet	$0.74^{+0.22}_{-0.20}$	125.6	97%	3%	0%	0%
VBF tag	$0.60^{+0.57}_{-0.46}$	125.6	17%	83%	0%	0%
Vh tag	$0.39^{+1.97}_{-1.87}$	125.6	0%	0%	100%	0%
Wh tag	$0.56^{+1.27}_{-0.95}$	125.6	0%	0%	100%	0%
Tevatron (10.0 fb^{-1} at 1.96 TeV) [133]						
Combined	$0.85^{+0.88}_{-0.81}$	125	78%	5%	17%	0%

TABLE IV. Data on signal strengths of $h \to b\bar{b}$ recorded by ATLAS Collaboration, CMS Collaboration, and Tevatron. The percentages of each production mode in each data are given.

			Production mode			
Channel	Signal strength μ	m_h (GeV)	ggF	VBF	Vh	tth
ATLAS (4.7 fb^{-1} at 7 TeV + 20.3 fb^{-1} at 8 TeV) [137]						
Vh tag	0.52 ± 0.4	125.36	0%	0%	100%	0%
CMS (up to 5.1 fb^{-1} at 7 TeV + 18.9 fb^{-1} at 8 TeV) [138]						
Vh tag	1.0 ± 0.5	125.8	0%	0%	100%	0%
Tevatron (10.0 fb^{-1} at 1.96 TeV) [133]						
Vh tag	$1.56^{+0.72}_{-0.73}$	125	0%	0%	100%	0%

TABLE V. Data on signal strengths of $h \to \tau^+\tau^-$ recorded by ATLAS and CMS Collaborations. The percentages of each production mode in each data are given. For ATLAS Collaboration data, we use a correlation of $\rho = -0.5$.

			Production mode			
Channel	Signal strength μ	m_h (GeV)	ggF	VBF	Vh	tth
ATLAS (4.5 fb^{-1} at 7 TeV + 20.3 fb^{-1} at 8 TeV) [139]						
$\mu(ggF)$	$1.93^{+1.42}_{-1.11}$	125.36	100%	0%	0%	0%
$\mu(VBF + VH)$	$1.24^{+0.57}_{-0.53}$	125.36	0%	59.4%	40.6%	
CMS (up to 4.9 fb^{-1} at 7 TeV + 19.7 fb^{-1} at 8 TeV) [140]						
0 jet	0.34 ± 1.09	125	96.9%	1.0%	2.1%	0%
1 jet	1.07 ± 0.46	125	75.7%	14.0%	10.3%	0%
VBF tag	0.95 ± 0.41	125	19.6%	80.4%	0%	0%
Vh tag	-0.33 ± 1.02	125	0%	0%	100%	0%

TABLE VI. Data on signal strengths for various decay modes of the Higgs boson which is produced through the $t\bar{t}h$ production mode, for both ATLAS and CMS. Note that, in the various analyses, contaminations from other production modes are negligible.

			Production mode			
Channel	Signal strength μ	m_h (GeV)	ggF	VBF	Vh	tth
ATLAS (4.5 fb^{-1} at 7 TeV + 20.3 fb^{-1} at 8 TeV) [48]						
$\gamma\gamma$	$1.3^{2.62}_{-1.72}$	125.4	0%	0%	0%	100%
ATLAS (20.3 fb^{-1} at 8 TeV) [63]						
$b\bar{b}$	$+1.5^{+1.1}_{-1.1}$	125	0%	0%	0%	100%
CMS (up to 5.1 fb^{-1} at 7 TeV + 19.7 fb^{-1} at 8 TeV) [50]						
$\gamma\gamma$	$2.7^{2.6}_{-1.8}$	125.6	0%	0%	0%	100%
$b\bar{b}$	$+0.7^{+1.9}_{-1.9}$	125.6	0%	0%	0%	100%
$\tau_h\tau_h$	$-1.3^{+6.3}_{-5.5}$	125.6	0%	0%	0%	100%
4-lepton	$-4.7^{+5.0}_{-1.3}$	125.6	0%	0%	0%	100%
3-lepton	$+3.1^{+2.4}_{-2.0}$	125.6	0%	0%	0%	100%
Same-sign 2l	$+5.3^{+2.1}_{-1.8}$	125.6	0%	0%	0%	100%
ATLAS (20.3 fb^{-1} at 8 TeV) [64,65]						
2lepton0$\tau_{\rm had}$	$2.8^{2.1}_{-1.9}$	125.0	0%	0%	0%	100%
3-lepton	$+2.8^{+2.2}_{-1.8}$	125.0	0%	0%	0%	100%
2lepton1$\tau_{\rm had}$	$-0.9^{+3.1}_{-2.0}$	125.0	0%	0%	0%	100%
4-lepton	$1.8^{+6.9}_{-2.0}$	125.0	0%	0%	0%	100%
1lepton2$\tau_{\rm had}$	$-9.6^{+9.6}_{-9.7}$	125.0	0%	0%	0%	100%

Project "DMAstro-LHC", ANR-12-BS05-0006, for a visit to LAPTh.

APPENDIX A: DATA USED IN FITS

We present in the following Tables I to VI the data used in the fits.

APPENDIX B: FORM FACTORS

The loop functions that we have used in the text appear in the analytical expressions for the one-loop induced widths $h \to \gamma\gamma$ and $h \to gg$. Keeping only the dominant W and top contributions we have (see [66,67])

$$\Gamma_{\gamma\gamma} = \frac{G_F \alpha^2 m_h^3}{128\sqrt{2}\pi^3}\left\{\left|\kappa_W A_W^a(\tau_W) + \frac{4}{3} a_t A_t^a(\tau_t)\right|^2 + \left|\frac{4}{3} b_t A_t^b(\tau_t)\right|^2\right\},$$
$$\Gamma_{gg} = \frac{G_F \alpha_s^2 m_h^3}{64\sqrt{2}\pi^3}\{|a_t A_t^a(\tau_t)|^2 + |b_t A_t^b(\tau_t)|^2\}, \quad \text{(B1)}$$

where

$$A_t^a(\tau) = \frac{2}{\tau^2}(\tau + (\tau-1)f(\tau)),$$
$$A_W^a(\tau) = -\frac{1}{\tau^2}(2\tau^2 + 3\tau + 3(2\tau-1)f(\tau)),$$
$$A_t^b(\tau) = \frac{2}{\tau} f(\tau), \quad \text{(B2)}$$

with $\tau_i = \frac{m_h^2}{4m_i^2}$ and

$$f(\tau) = \begin{cases} \arcsin^2\sqrt{\tau} & \text{for } \tau \le 1 \\ -\frac{1}{4}\left[\log\frac{1+\sqrt{1-\tau^{-1}}}{1-\sqrt{1-\tau^{-1}}} - i\pi\right]^2 & \text{for } \tau > 1 \end{cases}. \quad \text{(B3)}$$

Since $\tau_t \ll 1$, an expansion of the loop functions $A_t^{a,b}$ in τ_t confirms that the departure from the infinite mass limit is very small. Indeed, we can write

$$A_t^a(\tau_t) = \frac{4}{3}\left(1 + \frac{7}{30}\tau_t + \mathcal{O}(\tau_t^2)\right),$$
$$A_t^b(\tau_t) = 2\left(1 + \frac{\tau_t}{3} + \mathcal{O}(\tau_t^2)\right). \quad \text{(B4)}$$

With $\tau_t = m_h^2/(4m_t^2) \simeq 0.15$, one sees that corrections to the amplitudes in the $\tau_t \to 0$ limit are, respectively, of order 3.5% and 5%.

[1] G. Aad *et al.* (ATLAS Collaboration), Phys. Lett. B **716**, 1 (2012).
[2] S. Chatrchyan *et al.* (CMS Collaboration), Phys. Lett. B **716**, 30 (2012).
[3] S. Chatrchyan *et al.* (CMS Collaboration), J. High Energy Phys. 06 (2013) 081.
[4] G. Aad *et al.* (ATLAS Collaboration), Phys. Lett. B **726**, 120 (2013).
[5] Technical Report No. ATLAS-CONF-2013-013 (CERN, Geneva, 2013).
[6] S. Chatrchyan *et al.* (CMS Collaboration), Phys. Rev. D **89**, 092007 (2014).
[7] S. Chatrchyan *et al.* (CMS Collaboration), Phys. Rev. Lett. **110**, 081803 (2013).
[8] S. Choi, D. Miller, M. Muhlleitner, and P. Zerwas, Phys. Lett. B **553**, 61 (2003).
[9] R. M. Godbole, D. Miller, and M. M. Muhlleitner, J. High Energy Phys. 12 (2007) 031.
[10] Y. Gao, A. V. Gritsan, Z. Guo, K. Melnikov, M. Schulze, and N. V. Tran, Phys. Rev. D **81**, 075022 (2010).
[11] A. De Rujula, J. Lykken, M. Pierini, C. Rogan, and M. Spiropulu, Phys. Rev. D **82**, 013003 (2010).
[12] D. Stolarski and R. Vega-Morales, Phys. Rev. D **86**, 117504 (2012).
[13] S. Bolognesi, Y. Gao, A. V. Gritsan, K. Melnikov, M. Schulze, N. V. Tran, and A. Whitbeck, Phys. Rev. D **86**, 095031 (2012).
[14] Y. Chen, A. Falkowski, I. Low, and R. Vega-Morales, Phys. Rev. D **90**, 113006 (2014).
[15] S. Chatrchyan *et al.* (CMS Collaboration), J. High Energy Phys. 01 (2014) 096.
[16] V. e. a. Khachatryan (CMS Collaboration), Technical Report No. CERN-PH-EP-2014-265, CMS-HIG-14-018-003, arXiv:1411.3441 (institution CERN, Geneva, 2014).
[17] S. Dawson, A. Gritsan, H. Logan, J. Qian, C. Tully *et al.*, arXiv:1310.8361.
[18] T. Plehn, D. L. Rainwater, and D. Zeppenfeld, Phys. Rev. Lett. **88**, 051801 (2002).
[19] V. Hankele, G. Klamke, D. Zeppenfeld, and T. Figy, Phys. Rev. D **74**, 095001 (2006).
[20] J. R. Andersen, K. Arnold, and D. Zeppenfeld, J. High Energy Phys. 06 (2010) 091.
[21] J. R. Andersen, V. Del Duca, and C. D. White, J. High Energy Phys. 02 (2009) 015.
[22] A. Djouadi, R. Godbole, B. Mellado, and K. Mohan, Phys. Lett. B **723**, 307 (2013).
[23] C. Englert, D. Goncalves-Netto, K. Mawatari, and T. Plehn, J. High Energy Phys. 01, (2013) 148.
[24] T. Han and Y. Li, Phys. Lett. B **683**, 278 (2010).
[25] N. D. Christensen, T. Han, and Y. Li, Phys. Lett. B **693**, 28 (2010).
[26] N. Desai, D. K. Ghosh, and B. Mukhopadhyaya, Phys. Rev. D **83**, 113004 (2011).
[27] J. Ellis, D. S. Hwang, V. Sanz, and T. You, J. High Energy Phys. 11 (2012) 134.
[28] R. M. Godbole, D. J. Miller, K. A. Mohan, and C. D. White, J. High Energy Phys. 04 (2015) 103.
[29] R. Godbole, D. J. Miller, K. Mohan, and C. D. White, Phys. Lett. B **730**, 275 (2014).
[30] C. Delaunay, G. Perez, H. de Sandes, and W. Skiba, Phys. Rev. D **89**, 035004 (2014).
[31] S. Berge, W. Bernreuther, and S. Kirchner, Eur. Phys. J. C **74**, 3164 (2014).
[32] S. Berge, W. Bernreuther, and H. Spiesberger, arXiv:1208.1507.
[33] S. Berge, W. Bernreuther, B. Niepelt, and H. Spiesberger, Phys. Rev. D **84**, 116003 (2011).
[34] S. Berge, W. Bernreuther, and J. Ziethe, Phys. Rev. Lett. **100**, 171605 (2008).
[35] A. Djouadi and G. Moreau, Eur. Phys. J. C **73**, 2512 (2013).
[36] K. Cheung, J. S. Lee, and P.-Y. Tseng, J. High Energy Phys. 05 (2013) 134.
[37] K. Cheung, J. S. Lee, E. Senaha, and P.-Y. Tseng, J. High Energy Phys. 06 (2014) 149.
[38] S. Biswas, E. Gabrielli, and B. Mele, J. High Energy Phys. 01 (2013) 088.
[39] S. Biswas, E. Gabrielli, F. Margaroli, and B. Mele, J. High Energy Phys. 07 (2013) 073.
[40] J. Ellis, D. S. Hwang, K. Sakurai, and M. Takeuchi, J. High Energy Phys. 04 (2014) 004.
[41] J. Yue, arXiv:1410.2701.
[42] J. Chang, K. Cheung, J. S. Lee, and C.-T. Lu, J. High Energy Phys. 05 (2014) 062.
[43] A. Kobakhidze, L. Wu, and J. Yue, J. High Energy Phys. 10 (2014) 100.
[44] C. Englert and E. Re, Phys. Rev. D **89**, 073020 (2014).
[45] Technical Report No. CMS-PAS-HIG-14-001 (CERN, Geneva, 2014).
[46] Technical Report No. CMS-PAS-HIG-14-015 (CERN, Geneva, 2014).
[47] Technical Report No. CMS-PAS-HIG-14-026 (CERN, Geneva, 2015).
[48] G. Aad *et al.* (ATLAS Collaboration), Phys. Lett. B **740**, 222 (2015).
[49] Technical Report No. ATLAS-CONF-2014-011 (CERN, Geneva, 2014).
[50] V. Khachatryan *et al.* (CMS Collaboration), J. High Energy Phys. 09 (2014) 087.
[51] Technical Report No. ATL-PHYS-PUB-2014-012 (CERN, Geneva, 2014).
[52] T. Plehn, G. P. Salam, and M. Spannowsky, Phys. Rev. Lett. **104**, 111801 (2010).
[53] P. Artoisenet, P. de Aquino, F. Maltoni, and O. Mattelaer, Phys. Rev. Lett. **111**, 091802 (2013).
[54] M. R. Buckley, T. Plehn, T. Schell, and M. Takeuchi, J. High Energy Phys. 02 (2014) 130.
[55] F. Maltoni, D. L. Rainwater, and S. Willenbrock, Phys. Rev. D **66**, 034022 (2002).
[56] D. Curtin, J. Galloway, and J. G. Wacker, Phys. Rev. D **88**, 093006 (2013).
[57] P. Agrawal, S. Bandyopadhyay, and S. P. Das, Phys. Rev. D **88**, 093008 (2013).
[58] D. Stockinger, J. Phys. G **34**, R45 (2007).
[59] J. Brod, U. Haisch, and J. Zupan, J. High Energy Phys. 11 (2013) 180.
[60] A. Arbey, J. Ellis, R. Godbole, and F. Mahmoudi, Eur. Phys. J. C **75**, 85 (2015).

[61] Technical Report No. CMS-PAS-HIG-14-009 (CERN, Geneva, 2014).
[62] Technical Report No. ATLAS-CONF-2014-009 (CERN, Geneva, 2014).
[63] G. Aad *et al.* (ATLAS Collaboration), arXiv:1503.05066.
[64] Technical Repot No. ATLAS-CONF-2015-006 (CERN, Geneva, 2015).
[65] G. Aad *et al.* (ATLAS), arXiv:1506.05988.
[66] A. Djouadi, Phys. Rep. **459**, 1 (2008).
[67] M. Spira, A. Djouadi, D. Graudenz, and P. Zerwas, Nucl. Phys. **B453**, 17 (1995).
[68] G. Cacciapaglia, A. Deandrea, G. D. La Rochelle, and J.-B. Flament, J. High Energy Phys. 03 (2013) 029.
[69] S. Banerjee, S. Mukhopadhyay, and B. Mukhopadhyaya, J. High Energy Phys. 10 (2012) 062.
[70] G. Bhattacharyya, D. Das, and P. B. Pal, Phys. Rev. D **87**, 011702 (2013).
[71] D. Choudhury, R. Islam, and A. Kundu, Phys. Rev. D **88**, 013014 (2013).
[72] Technical Report No. CMS-PAS-HIG-13-005 (CERN, Geneva, 2013).
[73] Technical Report No. ATLAS-CONF-2013-034 (CERN, Geneva, 2013).
[74] K. Nishiwaki, S. Niyogi, and A. Shivaji, J. High Energy Phys. 04 (2014) 011.
[75] ATLAS Collaboration, ATLAS detector and physics performance: Technical Design Report, available on atlas.web.cern.ch.
[76] G. Bayatian *et al.* (CMS Collaboration), J. Phys. G **34**, 995 (2007).
[77] G. Aarons *et al.* (ILC), arXiv:0709.1893.
[78] A. Djouadi, J. Kalinowski, and P. Zerwas, Mod. Phys. Lett. A **07**, 1765 (1992).
[79] A. Djouadi, J. Kalinowski, and P. Zerwas, Z. Phys. C **54**, 255 (1992).
[80] B. Grzadkowski, J. F. Gunion, and J. Kalinowski, Phys. Rev. D **60**, 075011 (1999).
[81] S. Dawson and L. Reina, Phys. Rev. D **57**, 5851 (1998).
[82] S. Dittmaier, M. Kramer, Y. Liao, M. Spira, and P. Zerwas, Phys. Lett. B **441**, 383 (1998).
[83] Y. You, W.-G. Ma, H. Chen, R.-Y. Zhang, S. Yan-Bin, and H.-S. Hou, Phys. Lett. B **571**, 85 (2003).
[84] G. Belanger, F. Boudjema, J. Fujimoto, T. Ishikawa, T. Kaneko, K. Kato, Y. Shimizu, and Y. Yasui, Phys. Lett. B **571**, 163 (2003).
[85] S. Bar-Shalom, D. Atwood, G. Eilam, R. Mendel, and A. Soni, Phys. Rev. D **53**, 1162 (1996).
[86] D. Atwood, S. Bar-Shalom, G. Eilam, and A. Soni, Phys. Rep. **347**, 1 (2001).
[87] J. F. Gunion, B. Grzadkowski, and X.-G. He, Phys. Rev. Lett. **77**, 5172 (1996).
[88] P. Bhupal Dev, A. Djouadi, R. Godbole, M. Muhlleitner, and S. Rindani, Phys. Rev. Lett. **100**, 051801 (2008).
[89] R. Godbole, C. Hangst, M. Muhlleitner, S. Rindani, and P. Sharma, Eur. Phys. J. C **71**, 1681 (2011).
[90] R. Godbole, P. Bhupal Dev, A. Djouadi, M. Muhlleitner, and S. Rindani, *TOP08*, eConf C0705302 (2007).
[91] C.-S. Huang and S.-h. Zhu, Phys. Rev. D **65**, 077702 (2002).
[92] B. Ananthanarayan, S. K. Garg, J. Lahiri, and P. Poulose, Phys. Rev. D **87**, 114002 (2013).
[93] B. Ananthanarayan, S. K. Garg, C. Kim, J. Lahiri, and P. Poulose, Phys. Rev. D **90**, 014016 (2014).
[94] F. Demartin, F. Maltoni, K. Mawatari, B. Page, and M. Zaro, Eur. Phys. J. C **74**, 3065 (2014).
[95] R. Frederix, S. Frixione, V. Hirschi, F. Maltoni, R. Pittau, and P. Torrielli, Phys. Lett. B **701**, 427 (2011).
[96] E. Accomando, A. Akeroyd, E. Akhmetzyanova, J. Albert, A. Alves *et al.*, arXiv:hep-ph/0608079.
[97] R. Godbole, S. Kraml, M. Krawczyk, D. Miller, P. Niezurawski *et al.*, arXiv:hep-ph/0404024.
[98] J. F. Gunion and X.-G. He, Phys. Rev. Lett. **76**, 4468 (1996).
[99] X.-G. He, G.-N. Li, and Y.-J. Zheng, arXiv:1501.00012.
[100] S. Khatibi and M. M. Najafabadi, Phys. Rev. D **90**, 074014 (2014).
[101] D. Atwood and A. Soni, Phys. Rev. D **45**, 2405 (1992).
[102] J. Alwall, R. Frederix, S. Frixione, V. Hirschi, F. Maltoni, O. Mattelaer, H.-S. Shao, T. Stelzer, P. Torrielli, and M. Zaro, J. High Energy Phys. 07 (2014) 079.
[103] J. Pumplin, D. R. Stump, J. Huston, H.-L. Lai, P. Nadolsky, and Wu-Ki Tung, J. High Energy Phys. 07 (2002) 012.
[104] W. Beenakker, S. Dittmaier, M. Krämer, B. Plümper, M. Spira, and P. M. Zerwas, Phys. Rev. Lett. **87**, 201805 (2001).
[105] W. Beenakker, S. Dittmaier, M. Krämer, B. Plümper, M. Spira, and P. M. Zerwas, Nucl. Phys. **B653**, 151 (2003).
[106] L. Reina and S. Dawson, Phys. Rev. Lett. **87**, 201804 (2001).
[107] S. Dawson, L. Orr, L. Reina, and D. Wackeroth, Phys. Rev. D **67**, 071503 (2003).
[108] S. Dittmaier, S. Dittmaier, C. Mariotti, G. Passarino, R. Tanaka *et al.*, Report No. 10.5170/CERN-2012-002, 2012.
[109] M. Garzelli, A. Kardos, C. Papadopoulos, and Z. Trocsanyi, Europhys. Lett. **96**, 11001 (2011).
[110] H. B. Hartanto, B. Jager, L. Reina, and D. Wackeroth, Phys. Rev. D **91**, 094003 (2015).
[111] Y. Zhang, W.-G. Ma, R.-Y. Zhang, C. Chen, and L. Guo, Phys. Lett. B **738**, 1 (2014).
[112] S. Frixione, V. Hirschi, D. Pagani, H. Shao, and M. Zaro, J. High Energy Phys. 09 (2014) 065.
[113] S. Hoeche, F. Krauss, N. Lavesson, L. Lonnblad, M. Mangano *et al.*, arXiv:hep-ph/0602031.
[114] J. Baglio, A. Djouadi, and R. Godbole, Phys. Lett. B **716**, 203 (2012).
[115] F. Boudjema and R. K. Singh, J. High Energy Phys. 07 (2009) 028.
[116] M. R. Buckley, H. Murayama, W. Klemm, and V. Rentala, Phys. Rev. D **78**, 014028 (2008).
[117] R. M. Godbole, S. D. Rindani, and R. K. Singh, J. High Energy Phys. 12 (2006) 021.
[118] H. Murayama, I. Watanabe, and K. Hagiwara, Technical Report No. KEK-91-11, 1992.
[119] G. Mahlon and S. J. Parke, Phys. Rev. D **81**, 074024 (2010).
[120] G. Mahlon and S. J. Parke, Phys. Rev. D **53**, 4886 (1996).
[121] G. Aad *et al.* (ATLAS Collaboration), Phys. Rev. Lett. **108**, 212001 (2012).
[122] CMS Collaboration, Report No. CMS-PAS-TOP-12-004.

[123] R. M. Godbole, S. D. Rindani, and R. K. Singh, Phys. Rev. D **67**, 095009 (2003).
[124] S. Heinemeyer *et al.* (LHC Higgs Cross Section Working Group), Report No. 10.5170/CERN-2013-004, 2013.
[125] S. Biswas, R. Frederix, E. Gabrielli, and B. Mele, J. High Energy Phys. 07 (2014) 020.
[126] G. Brooijmans, R. Contino, B. Fuks, F. Moortgat, P. Richardson *et al.*, arXiv:1405.1617.
[127] G. Aad *et al.* (ATLAS), J. High Energy Phys. 11 (2013) 031.
[128] B. Nachman (ATLAS Collaboration), arXiv:1409.0318.
[129] CMS Collaboration, Technical Report No. CMS-PAS-TOP-11-031 (CERN, Geneva, 2012).
[130] D. Krohn, M. D. Schwartz, T. Lin, and W. J. Waalewijn, Phys. Rev. Lett. **110**, 212001 (2013).
[131] K. Cheung, J. S. Lee, and P.-Y. Tseng (ATLAS Collaboration), Phys. Rev. D **90**, 095009 (2014).
[132] V. Khachatryan *et al.* (CMS Collaboration), Eur. Phys. J. C **74**, 3076 (2014).
[133] Tevatron New Physics Higgs Working Group and CDF and D0 Collaborations, arXiv:1207.0449.
[134] G. Aad *et al.* (ATLAS Collaboration), Phys. Rev. D **90**, 052004 (2014).
[135] G. Aad *et al.* (ATLAS Collaboration), Phys. Rev. D **91**, 012006 (2015).
[136] Technical Report No. ATLAS-CONF-2014-060 (CERN, Geneva, 2014).
[137] G. Aad *et al.* (ATLAS Collaboration), J. High Energy Phys. 01 (2015) 069.
[138] S. Chatrchyan *et al.* (CMS Collaboration), Phys. Rev. D **89**, 012003 (2014).
[139] Technical Report No. ATLAS-CONF-2014-061 (CERN, Geneva, 2014).
[140] S. Chatrchyan *et al.* (CMS Collaboration), J. High Energy Phys. 05 (2014) 104.